Impact of the Precursor Gas Ratio on Dispersion Engineering of Broadband Silicon Nitride Microresonator Frequency Combs

GREGORY MOILLE[1,2*], DARON WESTLY[2], GREGORY SIMELGOR[2], AND KARTIK SRINIVASAN[1,2]

[1] *Joint Quantum Institute, NIST/University of Maryland, College Park, USA*
[2] *Microsystems and Nanotechnology Division, National Institute of Standards and Technology, Gaithersburg, USA*
[*] *Corresponding author: gmoille@umd.edu*

2021-12-07

Microresonator frequency combs, or microcombs, have gained wide appeal for their rich nonlinear physics and wide range of applications. Stoichiometric silicon nitride films grown via low-pressure chemical vapor deposition (LPCVD), in particular, are widely used in chip-integrated Kerr microcombs. Critical to such devices is the ability to control the microresonator dispersion, which has contributions from both material refractive index dispersion and geometric confinement. Here, we show that modifications to the ratio of the gaseous precursors in LPCVD growth has a significant impact on material dispersion and hence the overall microresonator dispersion. In contrast to the many efforts focused on comparison between Si-rich films and stoichiometric (Si_3N_4) films, here we focus on films whose precursor gas ratios should nominally place them in the stoichiometric regime. We further show that microresonator geometric dispersion can be tuned to compensate for changes in the material dispersion.

The ability to realize frequency comb generation in integrated photonic platforms through dissipative Kerr soliton (DKS) formation in $\chi^{(3)}$ microresonators has opened up numerous applications in timekeeping, communications, and spectroscopy [1]. Recent demonstrations combining DKS microcombs with chip-scale lasers [2, 3], to the extent of realizing octave-spanning bandwidth [4], highlight the potential for field deployment of such systems. This is particularly true for silicon nitride (SiN), which not only has been utilized in numerous demonstrations [5], but has been shown to fit within foundry-like fabrication process flows suitable for mass production [6]. Successful use of SiN within applications hinges on its large Kerr nonlinearity, broadband optical transparency, and reproducible and controllable dispersion, the latter being particularly critical for broadband applications such as the generation of octave-spanning combs [7–10]. The microcomb bandwidth and shape is entirely defined through the resonator dispersion, which can be decomposed in two elements: the material dispersion and the geometric dispersion (fig. 1), the former defined during the material growth, and the latter relying on accurate dimensions of the resonator compared to the theoretical design [11]. SiN growth for microcombs is typically done via low pressure chemical vapor deposition (LPCVD) using two precursor gases, ammonia (NH_3) and dichlorosilane (DCS or SiH_2Cl_2), where for fixed other conditions, the ratio between these two gases defines the composition of the deposited film. Most Kerr comb works have focused on achieving stoichiometric films, i.e., Si_3N_4, though a substantial amount of work has been conducted in studying silicon rich films [12–15], in part due to the higher nonlinear coefficient in this regime, with its refractive index dispersion also having been thoroughly studied [13]. Yet, stoichiometric films are often preferred due to linear losses that are typically lower and a wider optical transparency window, the latter of particular importance considering the possibility of nonlinear absorption. Interestingly, for a given pressure, temperature, and total gas flow, the gas ratio between NH_3 and DCS at which the stoichiometry condition is reached remains unclear; in the microcomb literature, NH_3:DCS $> 2:1$ has been cited [16], though larger NH_3:DCS ratios have also been considered [17, 18]. LPCVD studies have shown the film stoichiometry to remain largely unchanged up to a gas ratio of 30:1 [19, 20]. Here, we study LPCVD-deposited SiN films within this nominally stoichiometric regime with a NH_3:DCS gas ratio $> 2:1$. We find that the refractive index dispersion continues to change as the NH_3:DCS ratio is increased, with 3:1, 5:1, 7:1, and 15:1 ratios considered. We consider the impact of this varying material dispersion on the integrated dispersion of microresonators fabricated in these LPCVD-deposited films, and show through experimental generation of DKS microcomb states that differences in material dispersion between the films can be somewhat compensated through geometric dispersion, in particular, the thickness of the SiN film.

Growth of SiN is conducted through LPCVD onto a 3 µm thick silicon dioxide (SiO_2) layer that has been grown via thermal oxidation of a 100 mm silicon wafer. The precursor gases, as stated previously, are NH_3 and DCS, where the NH_3/DCS ratio is adjusted with a fixed DCS flow of 8.3×10^{-7} $m^3.s^{-1}$ (50 sccm). We use a fixed temperature of 775 °C and pressure of 300 Pa for all the different grown films. No post-growth annealing is performed on the films, which would be necessary to avoid excess losses due to N-H bonds at 1550 nm, but can

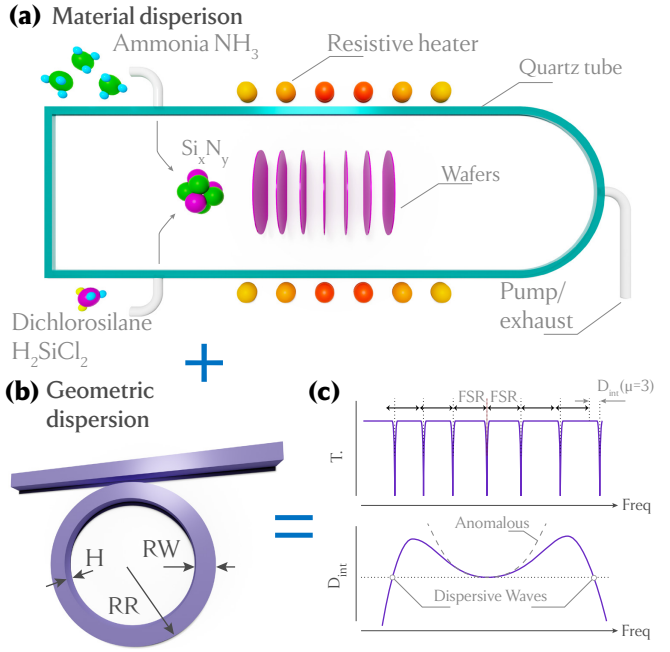

Fig. 1. **(a)** LPCVD system, where SiO_2 on Si wafers are loaded within a quartz furnace tube which is heated to a temperature of 775°C in our case. The two precursor gases are injected into the chamber at controllable flow levels. **(b)** Microring resonator were the three geometric parameters, ring radius RR, thickness H, and ring width RW determine the geometric dispersion contribution. **(c)** Both material and geometric dispersion contribute to the total dispersion of the resonator, allowing anomalous dispersion regime - free spectral range increasing with the frequency (upper panel), which also determines the spectral position of dispersive waves, appearing at the zero-crossings of the integrated dispersion (lower panel).

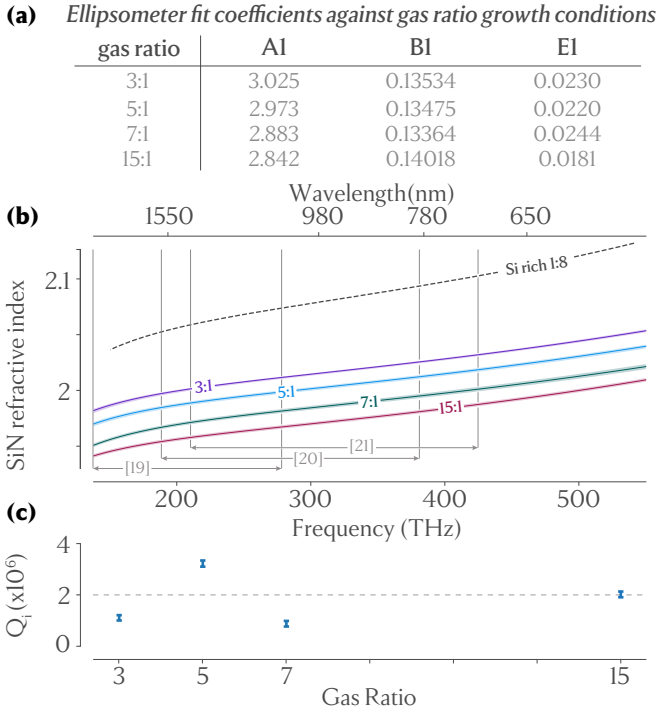

Fig. 2. **(a)** Ellipsometer fit coefficients for the different SiN varying gas ratio growth, where the films are deposited on silicon substrates and obtained from a the Sellmeier model. **(b)** Frequency-dependent refractive index for gas ratios of 3:1 (purple), 5:1 (cyan), 7:1 (teal) and 15:1 (red). The transparent areas account for an uncertainty of about 1% in the ellipsometer fitting coefficients. The Si-rich refractive index data (grey dashed) has been extracted from ref. [18]. The octave spanning frequency ranges for different experimental microcombs from refs[9, 21, 22] are indicated. **(c)** Average intrinsic quality factor taken over 12 resonances for each ring with the same geometry but created under different growth conditions. The displayed one standard deviation uncertainties are $\approx \pm 100 \times 10^3$.

be disregarded around our wavelength of interest at 1060 nm. In each growth run, we also use a Si wafer without SiO_2 as a reference, as this simpler layer structure limits the number of free parameters in fitting of ellipsometer measurements of the SiN thickness and refractive index. The ellipsometer measurements are performed over a wavelength range of 600 nm to 1700 nm, and are carried out for films grown with NH_3:DCS ratios of 3:1, 5:1, 7:1 and 15:1 (fig. 2(a)). We fit the ellipsometer measurements to a Sellmeier model, which has been found to be accurate for the SiN refractive index over a large bandwidth [23]

$$\varepsilon_{\mathrm{SiN}}(\lambda_\mu) = n^2_{\mathrm{SiN}}(\lambda_\mu) = 1 + A_1 \frac{\lambda_\mu^2}{\lambda_\mu^2 - B_1^2} - E_1 \lambda_\mu^2, \text{ with } \lambda_\mu = 10^6 c/f$$

being the wavelength in micrometers, and c and f being the speed of light and the frequency respectively. We note that other models have been used to fit ellipsometer measurements of SiN films taken over more extended infrared wavelengths [17]; however, as our concern in this work is the behavior in the near-infrared, the Sellmeier model is adequate. We note that the change in refractive index dispersion for differing gas ratios far exceeds in-wafer and run-to-run variation for a given gas ratio.

A clear trend appears where the larger the NH_3/DCS gas ratio, which corresponds to a lower proportion of silicon in the chemical process, the lower the refractive index, varying from around $n = 1.998$ and $n = 2.012$ to $n = 1.967$ and $n = 1.982$ at 193 THz and 283 THz (*i.e.* 1555 nm and 1060 nm) for 3:1 and 15:1 gas ratios, respectively (fig. 2(b)). Interestingly, Rutherford Backscattering Spectrometry (RBS) measurements do not show a change in the stoichiometry of the films for the different gas ratio (see supplementary material), and we measure a film stress of (1.1±0.1) GPa for each gas ratio, both of which are consistent with the literature [19, 20]. Although the material refractive index variation is important for resonator design to accomplish the desired dispersion for microcomb applications, it is also critical that the resonator intrinsic quality factor remain high, that is, that the differences in material growth do not result in added absorption. We fabricated microring resonators with ring radius $RR = 23$ µm, a SiN thickness of close to $H = 440$ nm, and a ring width $RW = 1060$ nm, in each of the SiN films, and performed linear transmission measurements of the resulting cavity in the 280 THz band, retrieving both the coupling and intrinsic quality factors [24]. The extracted average intrinsic quality factors (fig. 2(c)), which are in the 10^6 range, do not show a clear trend with precursor gas ratio. It is likely that the observed differences are due to process variation from run-to-run, rather than any specific attribute of the SiN films.

The cavity dispersion is composed of contributions from both geometric and material dispersion, and we next consider how

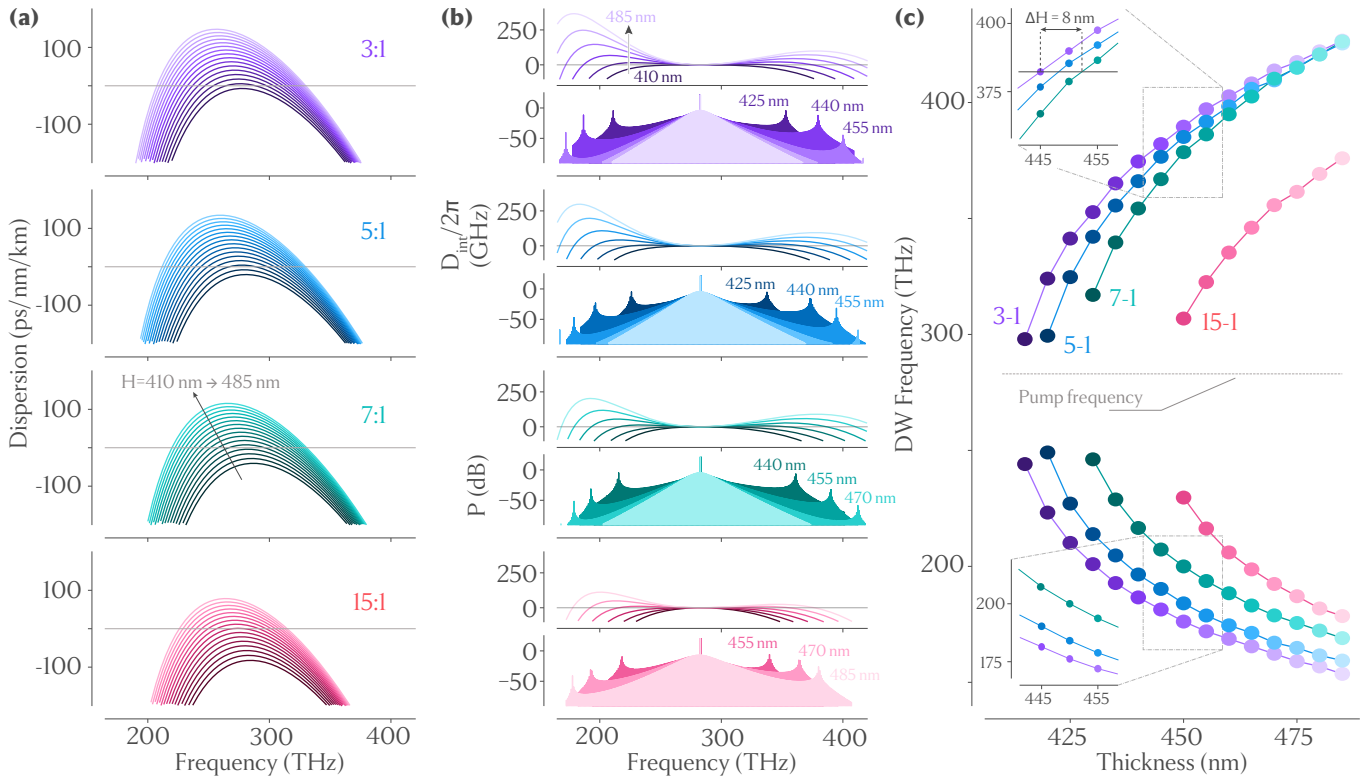

Fig. 3. **(a)** Numerical simulations of the dispersion parameter for a microring resonator with $RR = 23$ µm and $RW = 1060$ nm for a thickness that varies from 410 nm (darker) to 485 nm (lighter) considering different gas ratio, 3:1 (purple), 5:1 (cyan), 7:1 (teal) and 15:1 (red). **(b)** Integrated dispersion for the same set of geometries and gas ratios (top panel), with their corresponding LLE simulated spectra (bottom panel). **(c)** Position of the DWs, obtained from the zero-crossings of the integrated dispersion, as a function of thickness for the different gas ratios of interest, considering a pump frequency at 281 THz. The insets highlight the possibility to compensate for the DW shift due to the material dispersion by adjusting the geometric dispersion.

it is impacted by the variation in SiN precursor gas ratio. We use finite element method (FEM) simulations to compute the resonator dispersion characteristics for a variety of resonator geometries with different refractive index dispersion profiles based on the data from fig. 2. In this study, the microring with a $RR = 23$ µm ring radius and a $RW = 1060$ nm ring width is simulated with the thickness varied from $H = 410$ nm to $H = 485$ nm for the different gas ratios presented above. Because the refractive index is changed through the precursor gas ratio, for a fixed geometry - and hence a fixed geometric dispersion - the total ring dispersion is changed (fig. 3(a)). For example, the ring exhibit complete normal dispersion at a thickness below 410 nm for the 3:1 gas ratio and a thickness below 415 nm for the 5:1 gas ratio. The impact of the material dispersion is made more clear by studying the integrated dispersion, defined as the discrepancy between the cavity resonances and a fixed frequency grid defined by the free spectral range (FSR) around the pump, that is, $D_{\text{int}}(\mu) = \omega_{\text{res}} - (\omega_{\text{pmp}} + D_1\mu)$, with $\omega_{\text{res,pmp}}$ being the angular frequency of resonance and the pumped one respectively, $D_1 = 2\pi \times \text{FSR}$, and μ is the mode number relative to the pumped mode (*i.e* $\omega_{\text{res}}(\mu = 0) = \omega_{\text{pmp}}$). Studying the integrated dispersion (fig. 3(b)) allows for a more intuitive prediction of the supported DKS behavior, as $D_{\text{int}} = 0$ correspond to the location of DKS-induced dispersive waves (DWs), whose existence helps to broaden the comb spectrum beyond the anomalous dispersion window [5], and which can be tailored to aid in comb self-referencing [7]. From this standpoint, the impact of the material dispersion is obvious as it significantly modifies the frequency position of the DWs, exhibited through the integrated dispersion zero crossings and the resulting predicted comb spectra based on Lugiato-Lefever Eqaution (LLE) modeling [25]. For example, at the same thickness $H = 455$ nm, the high frequency DW exhibits a shift of 20 THz in moving from a 3:1 to 7:1 gas ratio, and the span decreases from 227 THz to close to 100 THz at 15:1 gas ratio. Interestingly, it is possible to at least partially compensate for changes in the material dispersion that arise from different growth conditions through appropriate adjustment of the geometric dispersion. For instance, it is possible to compensate for variations in the spectral position of one DW due to different gas ratios (fig. 3(c)) by adjusting the ring thickness. Nearly the same high frequency (short wavelength) DW can be obtained for any of the 3:1, 5:1, or 7:1 gas ratios, by adjusting the thickness between 445 nm and 453 nm. However, it is important to note that the thickness alone cannot compensate for shifts in the position of both DWs, and adjustments in the ring width would also be needed to provide the two-dimensional parameter space needed for such compensation.

To demonstrate such compensation of changes in material dispersion with adjustments to the geometric dispersion, we study two microring resonators with nominally identical in-plane dimensions, but different gas ratios were used in the SiN film growth (3:1 and 7:1), along with a thickness difference of about 10 nm (445 and 455 nm, respectively). Given our grown film thicknesses, comparison with a 15:1 gas ratio was not possible

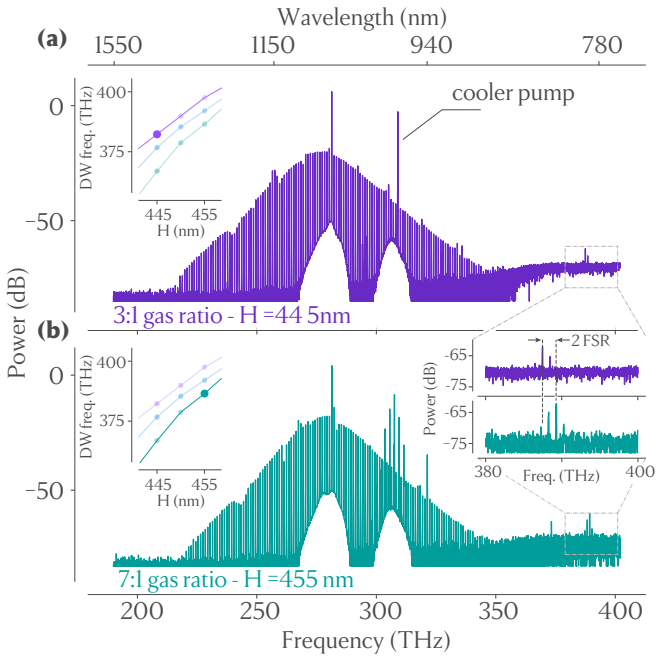

Fig. 4. DKS generated for the (a) 3:1 and (b) 7:1 gas ratios, exhibiting a short wavelength DW whose frequency matches to within 2 THz (right inset), as expected from the dispersion simulation presented in fig. 3(c) for each thickness (left insets).

as the microresonator remained in the normal dispersion regime. We pump both resonators around the same frequency of 281 THz (281.38 THz and 281.69 THz), corresponding to the same fist order transverse electric (TE_0) mode, with an in-waveguide power of $P_{\mathrm{pmp}} = 120$ mW. In order to reach the single soliton state, we actively cool the resonator by counterclockwise pumping a cross-polarized mode at a different frequency (307 THz or 977 nm), which has been demonstrated to allow adiabatic access to DKS states [10, 26]. The obtained DKS spectrum for each ring resonator exhibits almost the same high frequency DW (fig. 4(a)-(b)), to within 2 THz (i.e., a discrepancy of only 2 comb teeth) close to 385 THz, as predicted from LLE simulations where only the thickness and the material dispersion have been changed. In contrast, if the gas ratio was kept fixed (e.g., at 7:1), a 10 nm thickness change, from 445 nm to 455 nm, is predicted to result in a shift of the DW from approximately 355 THz to 385 THz corresponding to a ≈30 FSRs shift of the short wavelength DW.

In conclusion, we have demonstrated that although materials analysis studies have concluded that LPCVD growth can yield stoichiometric thin films for a wide range of precursor gas ratios, variation of the gas ratio within this regime continues to impact chromatic dispersion and its influence on microresonaor frequency comb generation. Although the change in material dispersion is not as dramatic as when moving to the silicon-rich regime, it is substantial enough to significantly impact the properties of broadband microresonator frequency combs. We further show that changes in geometric dispersion, for example resonator thickness, can be used to compensate for changes in material dispersion. Going forward, we believe our results point to the ability to use material growth conditions together with geometric control in the dispersion engineering of microresonators for broadband frequency comb applications.

Funding. Defense Advanced Research Projects Agency (DARPA-APHI); National Institute of Standards and Technology (NIST-on-a-chip). This work was performed in part at the Cornell NanoScale Facility, which is supported by the National Science Foundation (Grant NNCI-2025233).

Disclosures. The authors declare no conflicts of interest.

REFERENCES

1. S. A. Diddams, K. Vahala, and T. Udem, Science **369**, eaay3676 (2020).
2. B. Stern, X. Ji, Y. Okawachi, A. L. Gaeta, and M. Lipson, Nature **562**, 401 (2018).
3. C. Xiang, J. Liu, J. Guo, L. Chang, R. N. Wang, W. Weng, J. Peters, W. Xie, Z. Zhang, J. Riemensberger, J. Selvidge, T. J. Kippenberg, and J. E. Bowers, Science **373**, 99 (2021).
4. T. C. Briles, S.-P. Yu, L. Chang, C. Xiang, J. Guo, D. Kinghorn, G. Moille, K. Srinivasan, J. E. Bowers, and S. B. Papp, APL Photonics **6**, 026102 (2021).
5. A. L. Gaeta, M. Lipson, and T. J. Kippenberg, Nature Photonics **13**, 158 (2019).
6. J. Liu, G. Huang, R. N. Wang, J. He, A. S. Raja, T. Liu, N. J. Engelsen, and T. J. Kippenberg, Nature Communications **12**, 2236 (2021).
7. Q. Li, Q. Li, T. C. Briles, D. A. Westly, J. R. Stone, B. R. Ilic, S. A. Diddams, S. B. Papp, and K. Srinivasan, in "Frontiers in Optics 2015 (2015)," (Optical Society of America, 2015), p. FW6C.5.
8. M. H. P. Pfeiffer, C. Herkommer, J. Liu, H. Guo, M. Karpov, E. Lucas, M. Zervas, and T. J. Kippenberg, Optica **4**, 684 (2017).
9. S.-P. Yu, T. C. Briles, G. T. Moille, X. Lu, S. A. Diddams, K. Srinivasan, and S. B. Papp, Physical Review Applied **11**, 044017 (2019).
10. G. Moille, E. F. Perez, A. Rao, X. Lu, Y. Chembo, and K. Srinivasan, arXiv:2102.00301 [physics] (2021).
11. G. Moille, D. Westly, N. G. Orji, and K. Srinivasan, Applied Physics Letters **119**, 121103 (2021).
12. M. R. Dizaji, C. J. Krückel, A. Fülöp, P. A. Andrekson, V. Torres-Company, and L. R. Chen, Optics Express **25**, 12100 (2017).
13. C. J. Krückel, A. Fülöp, T. Klintberg, J. Bengtsson, P. A. Andrekson, and V. Torres-Company, Optics Express **23**, 25827 (2015).
14. D. T. H. Tan, K. J. A. Ooi, and D. K. T. Ng, Photonics Research **6**, B50 (2018).
15. Z. Ye, A. Fülöp, Ó. B. Helgason, P. A. Andrekson, and V. Torres-Company, Optics Letters **44**, 3326 (2019).
16. H. E. Dirani, A. Kamel, M. Casale, S. Kerdiles, C. Monat, X. Letartre, M. Pu, L. K. Oxenløwe, K. Yvind, and C. Sciancalepore, Applied Physics Letters **113**, 081102 (2018).
17. K. Luke, Y. Okawachi, M. R. E. Lamont, A. L. Gaeta, and M. Lipson, Optics Letters **40**, 4823 (2015).
18. Y. Xuan, Y. Liu, L. T. Varghese, A. J. Metcalf, X. Xue, P.-H. Wang, K. Han, J. A. Jaramillo-Villegas, A. Al Noman, C. Wang, S. Kim, M. Teng, Y. J. Lee, B. Niu, L. Fan, J. Wang, D. E. Leaird, A. M. Weiner, and M. Qi, Optica **3**, 1171 (2016).
19. P. Pan and W. Berry, J. Electrochem. Soc. **132**, 6 (1985).
20. V. J. Kapoor and R. S. Bailey, J. Electrochem. Soc. **137**, 9 (1990).
21. D. T. Spencer, T. Drake, T. C. Briles, J. Stone, L. C. Sinclair, C. Fredrick, Q. Li, D. Westly, B. R. Ilic, A. Bluestone, N. Volet, T. Komljenovic, L. Chang, S. H. Lee, D. Y. Oh, M.-G. Suh, K. Y. Yang, M. H. P. Pfeiffer, T. J. Kippenberg, E. Norberg, L. Theogarajan, K. Vahala, N. R. Newbury, K. Srinivasan, J. E. Bowers, S. A. Diddams, and S. B. Papp, Nature **557**, 81 (2018).
22. G. Moille, X. Lu, A. Rao, D. Westly, and K. Srinivasan, in "2020 Conference on Lasers and Electro-Optics (CLEO)," (2020), pp. 1–2.
23. W. Sellmeier, Annalen der Physik und Chemie **223**, 386 (1872).
24. M. Borselli, T. J. Johnson, and O. Painter, Optics Express **13**, 1515 (2005).
25. G. Moille, Q. Li, L. Xiyuan, and K. Srinivasan, Journal of Research of the National Institute of Standards and Technology **124**, 124012 (2019).
26. H. Zhou, Y. Geng, W. Cui, S.-W. Huang, Q. Zhou, K. Qiu, and C. Wei Wong, Light: Science & Applications **8**, 50 (2019).

FULL REFERENCES

1. S. A. Diddams, K. Vahala, and T. Udem, "Optical frequency combs: Coherently uniting the electromagnetic spectrum," Science **369**, eaay3676 (2020).
2. B. Stern, X. Ji, Y. Okawachi, A. L. Gaeta, and M. Lipson, "Battery-operated integrated frequency comb generator," Nature **562**, 401–405 (2018).
3. C. Xiang, J. Liu, J. Guo, L. Chang, R. N. Wang, W. Weng, J. Peters, W. Xie, Z. Zhang, J. Riemensberger, J. Selvidge, T. J. Kippenberg, and J. E. Bowers, "Laser soliton microcombs heterogeneously integrated on silicon," Science **373**, 99–103 (2021).
4. T. C. Briles, S.-P. Yu, L. Chang, C. Xiang, J. Guo, D. Kinghorn, G. Moille, K. Srinivasan, J. E. Bowers, and S. B. Papp, "Hybrid InP and SiN integration of an octave-spanning frequency comb," APL Photonics **6**, 026102 (2021).
5. A. L. Gaeta, M. Lipson, and T. J. Kippenberg, "Photonic-chip-based frequency combs," Nature Photonics **13**, 158–169 (2019).
6. J. Liu, G. Huang, R. N. Wang, J. He, A. S. Raja, T. Liu, N. J. Engelsen, and T. J. Kippenberg, "High-yield, wafer-scale fabrication of ultralow-loss, dispersion-engineered silicon nitride photonic circuits," Nature Communications **12**, 2236 (2021).
7. Q. Li, Q. Li, T. C. Briles, D. A. Westly, J. R. Stone, B. R. Ilic, S. A. Diddams, S. B. Papp, and K. Srinivasan, "Octave-spanning microcavity Kerr frequency combs with harmonic dispersive-wave emission on a silicon chip," in "Frontiers in Optics 2015 (2015)," (Optical Society of America, 2015), p. FW6C.5.
8. M. H. P. Pfeiffer, C. Herkommer, J. Liu, H. Guo, M. Karpov, E. Lucas, M. Zervas, and T. J. Kippenberg, "Octave-spanning dissipative Kerr soliton frequency combs in Si_3N_4 microresonators," Optica **4**, 684–691 (2017).
9. S.-P. Yu, T. C. Briles, G. T. Moille, X. Lu, S. A. Diddams, K. Srinivasan, and S. B. Papp, "Tuning Kerr-soliton frequency combs to atomic resonances," **11** (2019).
10. G. Moille, E. F. Perez, A. Rao, X. Lu, Y. Chembo, and K. Srinivasan, "Ultra-Broadband Soliton Microcomb Through Synthetic Dispersion," arXiv:2102.00301 [physics] (2021).
11. G. Moille, D. Westly, N. G. Orji, and K. Srinivasan, "Tailoring broadband kerr soliton microcombs via post-fabrication tuning of the geometric dispersion," Applied Physics Letters **119**, 121103 (2021).
12. M. R. Dizaji, C. J. Krückel, A. Fülöp, P. A. Andrekson, V. Torres-Company, and L. R. Chen, "Silicon-rich nitride waveguides for ultra-broadband nonlinear signal processing," Optics Express **25**, 12100–12108 (2017).
13. C. J. Krückel, A. Fülöp, T. Klintberg, J. Bengtsson, P. A. Andrekson, and V. Torres-Company, "Linear and nonlinear characterization of low-stress high-confinement silicon-rich nitride waveguides," Optics Express **23**, 25827–25837 (2015).
14. D. T. H. Tan, K. J. A. Ooi, and D. K. T. Ng, "Nonlinear optics on silicon-rich nitride - a high nonlinear figure of merit CMOS platform," Photonics Research **6**, B50–B66 (2018).
15. Z. Ye, A. Fülöp, Ó. B. Helgason, P. A. Andrekson, and V. Torres-Company, "Low-loss high-Q silicon-rich silicon nitride microresonators for Kerr nonlinear optics," Optics Letters **44**, 3326–3329 (2019).
16. H. E. Dirani, A. Kamel, M. Casale, S. Kerdiles, C. Monat, X. Letartre, M. Pu, L. K. Oxenløwe, K. Yvind, and C. Sciancalepore, "Annealing-free Si3N4 frequency combs for monolithic integration with Si photonics," Applied Physics Letters **113**, 081102 (2018).
17. K. Luke, Y. Okawachi, M. R. E. Lamont, A. L. Gaeta, and M. Lipson, "Broadband mid-infrared frequency comb generation in a Si_3N_4 microresonator," Optics Letters **40**, 4823–4826 (2015).
18. Y. Xuan, Y. Liu, L. T. Varghese, A. J. Metcalf, X. Xue, P.-H. Wang, K. Han, J. A. Jaramillo-Villegas, A. Al Noman, C. Wang, S. Kim, M. Teng, Y. J. Lee, B. Niu, L. Fan, J. Wang, D. E. Leaird, A. M. Weiner, and M. Qi, "High-Q silicon nitride microresonators exhibiting low-power frequency comb initiation," Optica **3**, 1171 (2016).
19. P. Pan and W. Berry, "The Composition and Physical Properties of LPCVD Silicon Nitride Deposited with Different N HJSiH 2Cl2Gas Ratios," J. Electrochem. Soc. **132**, 6 (1985).
20. V. J. Kapoor and R. S. Bailey, "Chemical Composition, Charge Trapping, and Memory Properties of Oxynitride Films for MNOS Devices," J. Electrochem. Soc. **137**, 9 (1990).
21. D. T. Spencer, T. Drake, T. C. Briles, J. Stone, L. C. Sinclair, C. Fredrick, Q. Li, D. Westly, B. R. Ilic, A. Bluestone, N. Volet, T. Komljenovic, L. Chang, S. H. Lee, D. Y. Oh, M.-G. Suh, K. Y. Yang, M. H. P. Pfeiffer, T. J. Kippenberg, E. Norberg, L. Theogarajan, K. Vahala, N. R. Newbury, K. Srinivasan, J. E. Bowers, S. A. Diddams, and S. B. Papp, "An optical-frequency synthesizer using integrated photonics," Nature **557**, 81–85 (2018).
22. G. Moille, X. Lu, A. Rao, D. Westly, and K. Srinivasan, "Post-processing dispersion engineering of frequency combs in microresonator addressing atomic clock," in "2020 Conference on Lasers and Electro-Optics (CLEO)," (2020), pp. 1–2.
23. W. Sellmeier, "Ueber die durch die Aetherschwingungen erregten Mitschwingungen der Körpertheilchen und deren Rückwirkung auf die ersteren, besonders zur Erklärung der Dispersion und ihrer Anomalien," Annalen der Physik und Chemie **223**, 386–403 (1872).
24. M. Borselli, T. J. Johnson, and O. Painter, "Beyond the Rayleigh scattering limit in high-Q silicon microdisks: Theory and experiment," Optics Express **13**, 1515–1530 (2005).
25. G. Moille, Q. Li, L. Xiyuan, and K. Srinivasan, "pyLLE: A Fast and User Friendly Lugiato-Lefever Equation Solver," Journal of Research of the National Institute of Standards and Technology **124**, 124012 (2019).
26. H. Zhou, Y. Geng, W. Cui, S.-W. Huang, Q. Zhou, K. Qiu, and C. Wei Wong, "Soliton bursts and deterministic dissipative Kerr soliton generation in auxiliary-assisted microcavities," Light: Science & Applications **8**, 50 (2019).